JOURNAL OF MATERIALS SCIENCE **38** (2003) 1589–1596

Failure probability of borosilicate glass under Hertz indentation load

RENTONG WANG*, N. KATSUBE‡
Department of Mechanical Engineering, Ohio State University, Columbus, OH 43210, USA
E-mail: katsube.1@osu.edu

R. R. SEGHI
College of Dentistry, Ohio State University, Columbus, OH 43210, USA

S. I. ROKHLIN
Department of Industrial, Welding and Systems Engineering, Ohio State University, Columbus, OH 43210, USA

The objective of this work is to test the hypothesis that the failure probability prediction model by Fischer-Cripps and Collins can be used without introducing an empirically derived parameter and therefore can serve as a predictive tool. We examined this hypothesis by Hertz cone crack initiation tests of flat borosilicate glass statically loaded through a spherical indenter. The Weibull parameters characterizing the surface flaw distribution were determined from biaxial flexure experiments using specimens with the same surface condition as in the indentation tests. Elastic moduli of the specimens were determined by using ultrasonic methods. In addition, the crack initiation was determined using stereo microscopy at 20× magnification.

The results demonstrated that the model can predict the minimum critical load and cumulative failure probability for small indenters within the 90% confidence level. Therefore, the current work demonstrates that the model can be used as a predictive tool provided the parameters necessary for the model accurately reflect those of the actual sample populations that are used for the experimental setup.

1. Introduction

When the flat surface of a brittle material is statically loaded through a spherical indenter, a cone crack forms at a critical load [1, 2]. When such experiments are repeated under identical conditions, the critical load data are known to show significant scatter. For small-radius indenters, Auerbach [3] experimentally observed that the average critical load, denoted by P_c, is proportional to the indenter radius R. This result is known as Auerbach's law. For large-radius indenters, P_c was observed to be approximately proportional to R^2 [4]. In addition, the cracks generally initiate at a radius 10 to 40% greater than the contact radius [5]. This percentage has been shown to increase as the ball radius R decreases [6].

The stress distribution within a specimen loaded through a spherical indenter was investigated by Hertz [1, 2] and Huber [7], and an extensive review of contact mechanics was given by Johnson [8]. Hertz-Huber stress fields show that the maximum tensile stress occurs at the edge of the contact area, and is proportional to the load, P, and inversely proportional to the square of the indenter radius, R. This implies that if the Griffith fracture criterion is used with the maximum tensile stress criterion, the theory predicts that the critical load, P_c, is proportional to R^2. This appears to contradict Auerbach's law for small indenters.

Frank and Lawn [9] applied the Griffith energy balance criterion for crack growth in the contact area by taking into consideration the rapid decrease of the tensile field with depth. Combining the Hertz-Huber stress field with the assumption that the crack path is along the σ_3 trajectory, they evaluated the strain energy release rate G for the crack path initiating at the contact radius a. Mouginot and Maugis [10] further developed the Frank and Lawn [9] theory by analyzing the possibility of crack initiation at various radii r_0 in the vicinity of the contact area. They showed that the minimum critical load corresponds to the relatively flat maximum of the envelope of the G-against-c/a curves for various starting radii r_0 (Fig. 3), and is proportional to the indenter radius R. This data provided a physical explanation of Auerbach's law.

Fischer-Cripps and Collins [11] and Fischer-Cripps [12] made significant progress with the model by

*Graduate student.
‡Author to whom all correspondence should be addressed.

combining the method developed by Mouginot and Maugis [10] with Weibull statistics. They assumed that the flaw size distribution could be described by Weibull statistics and predicted the cumulative failure probability as a function of load.

In comparing their predictions of the minimum critical load against the experimental data, they introduced a parameter that they described as being related to the contact friction that occurs between the indenter and the specimen surface. The value of this parameter was chosen so that an appropriate value of fracture surface energy could be used. While their methodology addresses the statistical variation of the experimental results with respect to the Griffith energy balance model, the empirical determination of this parameter limits the predictive capability of the theory developed. In addition, while this parameter was introduced to take into account friction, their own experimental data of spherical indentation tests on soda-lime glass with and without lubrication gave nearly identical results. Therefore, it raises the question of the true physical interpretation and necessity of this newly introduced parameter.

The objective of this work is to test the hypothesis that the method developed in [11, 12] can be used without an empirically derived parameter and therefore can serve as a predictive tool. We examined this hypothesis through indentation tests on borosilicate glass and careful reevaluation of the experimental procedure. We specifically focused on three potential sources of error. The value of Poisson's ratio greatly influences the theoretical prediction of the minimum critical indentation load. Therefore, Poisson's ratio was carefully measured using ultrasonic methods. Secondly, the ability to observe the moment of crack initiation can depend on the observation method and potentially influence the cumulative failure probability versus indentation load curves generated from this experimental data set. To address this concern, special attention was paid to the optical methods used to detect crack initiation. Finally, and perhaps most importantly, the Weibull parameters were determined from biaxial tests using the same specimen surface preparation as in the indentation tests. In order to take into account the multi-axial stress states, the fracture-mechanics-based statistical theory of Batdorf and coworkers [13, 14] was employed to determine Weibull parameters.

As a result, it was demonstrated that the model developed by Fischer-Cripps and Collins [11] and Fischer-Cripps [12] does not require the addition of an empirically derived parameter to adequately fit the experimental data of borosilicate glass. The method can be used to predict the minimum critical load and the cumulative failure probability versus load with a reasonable degree of accuracy.

2. Theoretical background

In this section, we briefly review the methodologies proposed in [11, 12], where flaw statistics with energy balance approaches are combined to describe the probability of Hertzian fracture. The basic formulation for indentation fracture of a flat brittle specimen loaded by a spherical indenter is summarized.

2.1. Minimum critical load determination

As shown schematically in Fig. 1, a Hertzian cone crack was observed to start slightly outside of the contact area when a flat brittle specimen was loaded by a spherical indenter. The rapidly changing axisymmetric stress field for Hertz spherical indentation on a semi-infinite space, known as the Hertz-Huber stress field, is summarized in the appendix. Outside the contact circle of radius a, the 1st principal stress is a tensile radial stress, and the 2nd principal stress is a compressive hoop stress. The 3rd principal stress at the surface is in the direction normal to the surface and is zero due to the stress free condition outside the contact circle (Fig. 1). Frank and Lawn [9] have proposed that the crack path is along the trajectory of the 3rd principal stress in the r-z plane, σ_3. The σ_3 trajectory is the curve whose tangents show the direction of σ_3 at the point of tangency. The motivation behind their work is that the crack growth should be orthogonal to the maximum tensile stress, and the known experimental results show the similarity between actual cone crack and the σ_3 trajectory.

Fig. 2 shows the maximum principal stress σ_1 plotted along the σ_3 stress trajectory (crack path shown in Fig. 1) for a different crack initiation parameter r_0/a, varying from 1.0 to 1.6. It is clear from Fig. 2 that the tensile stress diminishes very quickly below the

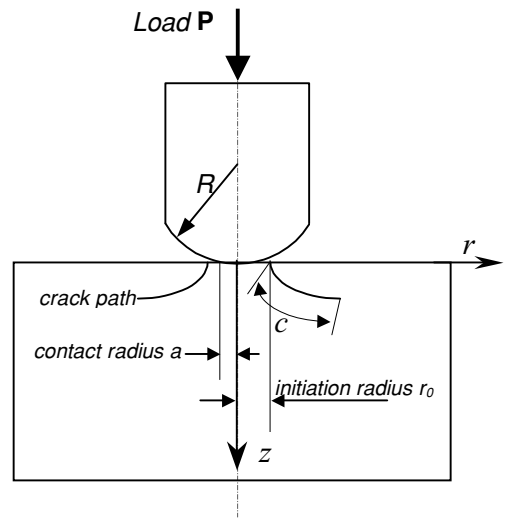

Figure 1 Hertzian cone crack.

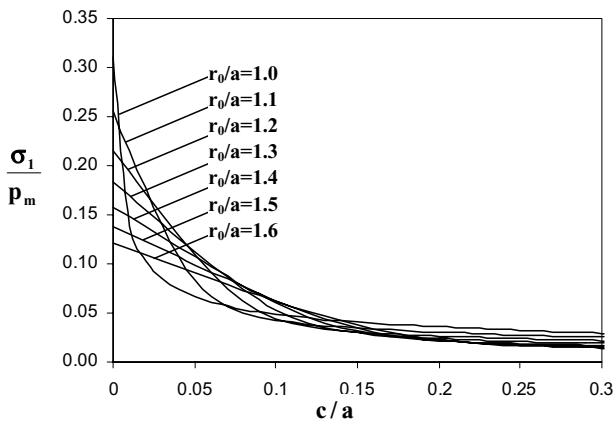

Figure 2 Principal stress σ in the r-z plane along crack paths initiated from different initiation radii r_0, a is contact radius. Poisson's ratio $\nu = 0.19$.

semi-infinite surface. In the well-known Griffith criterion for fracture, the surface energy for a new crack is related to the attendant release in strain energy, and the surface energy is expressed in terms of Irwin's stress intensity factor. Frank and Lawn [9] used the prior stress field without a crack to evaluate the stress intensity factor K_I assuming that a crack starts at the edge of the circle of contact, $r_0/a = 1$.

Mouginot and Maugis [10] modified the theoretical development by Frank and Lawn [9] by assuming that a crack can initiate with a range of starting radii in the neighborhood of the indenter. They also took into consideration the expanding crack front and evaluated the stress intensity factor K_I as follows

$$K_I = \frac{2}{\sqrt{\pi c}} \int_0^c \frac{r_b}{r_c} \frac{\sigma(b)}{\sqrt{1-(b/c)^2}} db \tag{1}$$

where the integral is calculated along the length of the proposed crack path b; c is the crack length; r_b and r_c are the radii of the crack at lengths b and c; and σ is the maximum principal stress in the prior stress field. Integrating the 1st principal stress (σ_1) distribution along the crack path (Fig. 2), the stress intensity factor K_I is obtained as a function of the flaw size c.

The strain energy release rate G for the plane strain assumption is given by

$$G = \frac{K_I^2(1-\nu^2)}{E}. \tag{2}$$

In the case of a spherical indenter, the well-known Hertz relation between the contact radius a, load P, and indenter radius R, is given by

$$a^3 = \frac{4kPR}{3E} \tag{3}$$

with

$$k = \frac{9}{16}\left[(1-\nu^2) + \frac{E}{E'}(1-\nu'^2)\right] \tag{4}$$

where the Young's modulus and Poisson's ratio of the specimen and those of the indenter are respectively denoted by E, ν, and E', ν'.

Combining Equations (1, 2, and 3), the strain energy release rate, G, can be expressed as

$$G = \frac{3(1-\nu^2)P}{\pi^3 kR}\phi(c/a) \tag{5}$$

where

$$\phi(c/a) = \frac{c}{a}\left[\int_0^{c/a} \frac{r_b}{r_c}\left(\frac{c^2}{a^2} - \frac{b^2}{a^2}\right)^{-1/2} f(b/a)d(b/a)\right]^2 \tag{6}$$

and

$$f(b/a) = \frac{\sigma(b/a)}{p_m}. \tag{7}$$

Note that a function ϕ is introduced so that the dependence of crack size, c, on the strain energy release rate, G, can be expressed in a non-dimensionalized form.

In Fig. 3, ϕ is plotted as a function of normalized crack length c/a for a range of starting radii r_0/a. As opposed to Frank and Lawn [9], where only one ϕ curve

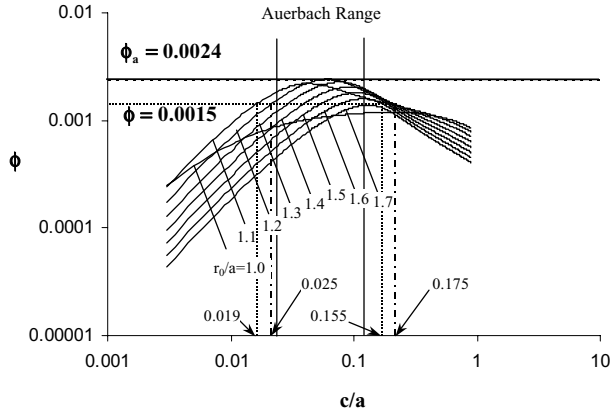

Figure 3 Strain energy release rate function ϕ as a function of normalized crack length c/a for different starting radii r_0/a.

with $r_0/a = 1$ was considered, Mouginot and Maugis [10] focused their attention on the envelope of ϕ for various values of r_0/a (Fig. 3). In particular, they noted that the envelope of ϕ reaches a plateau over a range of flaw sizes and argued that the crack will initiate and propagate at the minimum critical load P_a corresponding to the maximum value ϕ_a of the ϕ envelope under the condition of the existence of initial flaw sizes within this range. Using the crack growth criterion

$$G = 2\gamma \tag{8}$$

where γ is the surface energy, the minimum critical load P_a can be written as

$$P_a = \frac{k\pi^3(2\gamma)}{3(1-\nu^2)\phi_a}R \tag{9}$$

where ϕ_a is the maximum value of ϕ. By deriving Equation 9, Mouginot and Maugis [10] argued that the minimum critical load P_a is proportional to the indenter ball radius R. Therefore, they have shown that Auerbach's law (proportionality of the critical load to the indenter ball size) can be attributed not only to the diminishing stress field but also to the plateau for the envelope of the strain energy release rate for various starting radii.

2.2. Probability of failure under spherical contact loading

In analyzing Hertzian fracture, Fischer-Cripps and Collins [11] and Fischer-Cripps [12] combined the well-known Weibull distribution of critical flaw sizes with the fracture energy balance model of Mouginot and Maugis [10]. The Weibull parameters from Brown [15] were used [12] for data analysis. If the load applied on the indenter is less than the minimum critical load, P_a, there will be no crack initiating from the surface regardless of the flaw size since the Griffith fracture criterion is not met. If the applied load is higher than $P_a (P > P_a$ and $\phi = \phi_a P_a / P (< \phi_a))$, it is sufficient to satisfy the fracture criterion $G = 2\gamma$. The range of critical flaw size leading to crack initiation and propagation will depend on the crack initiation radius r_0. For example, in Fig. 3, given $\phi = 0.0015$, the range of critical flaw size

varies from $c/a = 0.019$ to 0.155 for a crack with starting radius $r/r_0 = 1.1$, while it varies from $c/a = 0.025$ to 0.175 for a crack with starting radius $r/r_0 = 1.2$.

Using the crack growth criterion

$$K_{IC} = \sigma\sqrt{\pi c}, \tag{10}$$

Fischer-Cripps [12] divided the surface area into N rings with inner radius r_i and width δr_i and calculated the probability to find at least one flaw with size larger than c_1 as

$$F_i(c > c_1) = 1 - \exp\left[-2k\pi r_i \delta r_i \left(\frac{K_{IC}}{\sqrt{\pi c_1}}\right)^m\right] \tag{11}$$

where i denotes the ith ring region and m and k are Weibull parameters.

The probability to find at least one flaw with size between c_1 and c_2 is given by

$$F^i(c_1 \le c \le c_2) = F_i(c > c_1) - F_i(c > c_2) \tag{12}$$

Therefore F^i is the probability of failure with crack initiation within the ith annular region.

The failure probability with crack initiation on the total surface area is then given by

$$F = 1 - \prod_{i=1}^{N}(1 - F^i) \tag{13}$$

3. Experimental setups

3.1. Material and samples preparation

Solid 15.9 mm borosilicate glass rods were sectioned with a slow speed diamond wheel saw (Leco VC-50, St Joseph, MI) under water coolant into 1.0 mm and 5.0 mm thick disks. The surfaces of the glass disks were sanded on a rotating wheel with 600 grit SiC sandpaper under water coolant. The disks were placed in distilled water and cleaned ultrasonically for 5 minutes prior to examination. The surfaces were examined under a binocular microscope at 15–20× magnification to assure a uniform finish. Any specimen surfaces that showed visible residual saw cuts were marked and re-sanded until a uniform surface finish was observed under the microscope.

3.2. Measurement of elastic properties

Elastic moduli of borosilicate glass were obtained by ultrasonic measurements of longitudinal $V_l = \sqrt{\frac{\lambda+2\mu}{\rho}}$ and shear $V_t = \sqrt{\frac{\mu}{\rho}}$ wave velocities, where λ is Lame's parameter and μ is the shear modulus. Young's modulus E is $E = \mu(3\lambda + 2\mu)/(\lambda + \mu)$. Density was measured by Archimedes method. The ultrasonic velocity measurements were performed at 10 MHz by the pulse-echo method by both immersion and contact techniques for longitudinal wave velocity and by the contact method for shear wave velocity. A Panametrics 5073 PR pulsar/receiver and a Hewlett Packard 54504-A 400 MHz digital oscilloscope were used for time delay measurements by the signal overlapping technique. The sample thickness was measured by a micrometer. The precision of measurement is limited by the flatness and parallelness of the sample surfaces and by the couplant effect for the shear wave velocity measurement. We estimate at least three correct digits in the determination of the Young's and shear moduli on our samples.

3.3. Biaxial experiment

In this work, we experimentally determine the Weibull parameters by using biaxial flexural tests as shown schematically in Fig. 4. The 1 mm thick disks were supported at the edge by a ring of bearings and loaded on the top center through a WC ball indenter with radius of 4.76 mm. The experiments were carried out on the Universal Testing Machine (Instron Model 4020, Canton, Mass.) at a crosshead speed of 0.01 mm/min. A total of 35 specimens were used to obtain the failure probability distribution. Under this configuration, cracks are initiated from the bottom surface, which is subjected to biaxial tensile stress. The fracture initiation loads, P, were recorded for each specimen and the data sorted by magnitude of failure load. The cumulative probability F_i of crack initiation at the ith fracture load P_i is assumed to be

$$F_i = i/(N + 1) \tag{14}$$

where N is the number of specimens.

3.4. Indentation test

Indentation tests were carried out using three WC indenters with radii of 1.59, 3.00 and 4.76 mm respectively on 5 mm thick glass disks. The specimens were loaded on a universal testing machine at a crosshead speed of 0.01 mm/min. A total of 20 specimens were tested for each of indenter ball size.

A binocular microscope (20×) was used to observe the initiation of cone cracks. The specimens were transilluminated with fiber optic lights from two different directions. The microscope was set up to view the specimen through the side of the polished transparent glass disk. During the observation, the load at which any sign of crack initiation was observed was recorded as the initiation failure load. The loading was further increased after the initiation of crack until a well-developed cone crack was formed, at which point unloading took place. As was done for the biaxial data, the crack initiation loads, P, were sorted in the order of their magnitudes and the cumulative probability F_i of crack initiation at the ith fracture load, P_i, was calculated from Equation 14.

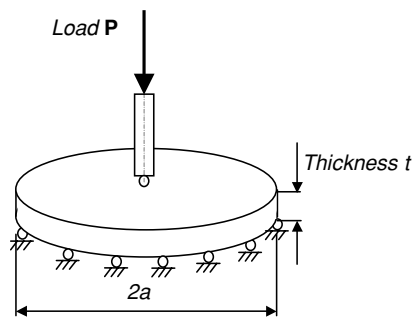

Figure 4 Biaxial flexure test.

4. Experimental results and analysis

In the data analysis, the Weibull parameters describing surface flaw distribution were determined by curve fitting of the biaxial tests data. The minimum failure loads for indentation tests with various radii of indenter balls were then predicted based on the theory summarized in section 2. From these results, the failure probability versus applied loads for the various spherical indenter sizes were predicted. The theoretical predictions are compared against the experimental indentation results (Fig. 6).

4.1. Determination of material parameters

4.1.1. Weibull parameters

Statistical theory for the brittle fracture of structures subjected to multiaxial loading has been developed by a number of researchers [13, 14, and 16]. Failure criteria based on the Griffith energy balance are combined with crack size and orientation in these theories. While there are some differences in the formulations of these fracture-mechanics-based theories, their equivalence for the case of identical flaw size distribution and fracture criterion has been demonstrated [17, 18]. This work employs these fracture-mechanics-based statistical theories for determination of Weibull parameters from the biaxial data.

Following Batdorf's formulation [13, 18], the cumulative probability of fracture, F, is given as

$$F = 1 - \exp\left[- \int_{\mathrm{A}} \int_0^{\infty} \frac{\Omega(\sigma, \sigma_{\mathrm{c}})}{2\pi} \frac{\mathrm{d}N(\sigma_{\mathrm{c}})}{\mathrm{d}\sigma_{\mathrm{c}}} \mathrm{d}\sigma_{\mathrm{c}} \mathrm{d}A \right] \tag{15}$$

where $\Omega(\sigma, \sigma_{\mathrm{c}})$ is a solid angle determined by the actual stress σ and critical stress σ_{c} according to the appropriate fracture criterion [18]. $N(\sigma_{\mathrm{c}})$ is the crack density as a function of σ_{c}, and it is assumed to be in the same form as in [18]:

$$N(\sigma_{\mathrm{c}}) = \bar{k} \sigma_{\mathrm{c}}^{\bar{\mathrm{m}}} \tag{16}$$

where $\bar{k}$ and $\bar{m}$ are the scale and shape parameters. In the case of a Ball-on-Ring test as shown in Fig. 4, the above probability F of cumulative failure (15) can be rewritten as

$$F = 1 - \exp\left[- \bar{k} \bar{m} a^2 I_{\mathrm{D}} \left(\frac{P}{\pi s^2} \right)^{\bar{\mathrm{m}}} \right] \tag{17}$$

where I_{D} and s are given by

$$I_{\mathrm{D}} = \int_0^1 \mathrm{d}(r/a) \int_0^{\infty} \Omega\left(\frac{r}{a} \right) \left(\frac{\sigma_{\mathrm{c}}}{P/\pi s^2} \right)^{\bar{\mathrm{m}}-1} \mathrm{d}\left(\frac{\sigma_{\mathrm{c}}}{P/\pi s^2} \right) \tag{18}$$

and

$$s = t \left(2 \ln \frac{3a}{t} \right)^{-1/2} \tag{19}$$

where a is the plate radius and t is thickness, Ω represents critical flaw angle which can be determined from the biaxial stress state and fracture-mechanics-based critical stress. A crack propagates only if its orientation falls in the range of Ω. A constant, s, is introduced for the purpose of non-dimensionalizing stress in Equation 17. It can be chosen arbitrarily as long as it has dimension of the length; in this work, Equation 19 is used.

We determine the distribution parameters $\bar{k}$ and $\bar{m}$ by curve fitting of the experimental data of F versus P with Equation 17. Taking advantage of the linearity between $\ln(-\ln(1 - F))$ and $\ln(P)$, simple linear regression is employed. In Fig. 5 the experimental data and the best fit obtained by the least squares method are presented. The values of $\bar{\mathrm{m}}$ and $\bar{k}$ were determined to be 4.917 and 2.482×10^{-11} mm$^{-2} \cdot$ MPa$^{-4.917}$ respectively.

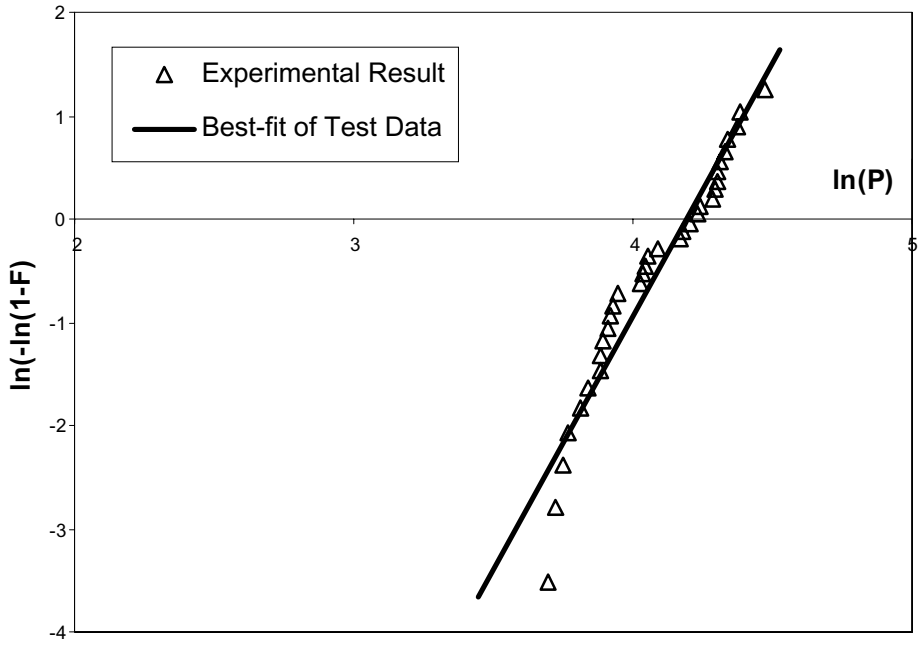

Figure 5 Best-fit biaxial test data to get Weibull parameters.

TABLE I Material properties

Young's modulus E	62.5 Gpa
Poisson's ratio ν	0.19
Surface energy γ	5.5 J · m^{-2}
Weibull parameters	
k	2.482×10^{-11} mm^{-2} · MPa$^{-4.917}$
m	4.917

For uniaxial tensile tests, Equation 15 reduces to the well-known Weibull equation

$$F(\sigma) = 1 - \exp(-kA\sigma^{\mathrm{m}}) \tag{20}$$

where A is the region under uniaxial tensile stress σ, and the Weibull parameters k and m in Equation 20 are expressed in terms of $\bar{k}$ and $\bar{m}$ as follows

$$k = \frac{1}{2\pi} I_{\mathrm{u}} \bar{m} \bar{k}; \quad m = \bar{m} \tag{21}$$

where

$$I_{\mathrm{u}} = \int_0^{\infty} \Omega(\sigma/\sigma_{\mathrm{c}})(\sigma/\sigma_{\mathrm{c}})^{\bar{\mathrm{m}}-1} \mathrm{d}(\sigma/\sigma_{\mathrm{c}}) \tag{22}$$

$\Omega(\sigma/\sigma_{\mathrm{c}})$ is determined from the uniaxial stress state and the fracture-mechanics-based critical stress as was done in the biaxial tests.

Based on the values of $\bar{m}$ and $\bar{k}$, the values of m and k were determined from Equations 21 and 22 and summarized in Table I.

4.1.2. Elastic moduli and surface energy

Young's modulus E and Poisson's ratio ν were measured ultrasonically as described in section 3.3 and are listed in Table I. The surface energy γ for borosilicate glass was taken from [19, 20], where it was obtained from the measured critical stress intensity factor K_{Ic}.

TABLE II Minimum critical load for 3 sizes of indenter balls

Indenter ball radius (mm)	1.59	3.00	4.76
Minimum critical load (N)	42.4	79.9	126.8

4.2. Indentation test analysis

4.2.1. The minimum critical load for fracture initiation

From a set of curves for ϕ versus normalized crack length for different starting radii (Fig. 3), the maximum value ϕ_{a} was determined to be 0.0024. Using this value in Equation 9, the minimum critical load was calculated for indenter ball radii of 1.59, 3.00 and 4.76 mm. The results are tabulated in Table II.

4.2.2. Indentation test results

Under indentation load the following sequence of events is observed. At a certain critical load, a ring crack begins to appear. Once the ring is completely formed, it propagates very slowly with increase of load and eventually develops into a well-developed cone crack. If at this moment one begins to decrease the load the crack often seems to disappear upon unloading. This observation suggests time dependent material behavior. This also indicates that it is very important to conduct *in situ* observation in order to capture the true crack initiation. The crack initiation loads were determined as described in section 3.4.

Based on the methods described in section 2 and the material parameters summarized in Table I, the cumulative failure probability beyond the minimum critical load was calculated. The minimum critical loads (zero failure probability) listed in Table II and the cumulative probability distributions obtained are plotted as solid lines in Fig. 6. The cumulative probability of failure for experimental data is obtained based on the method of median ranks. The corresponding 90% symmetric confidence intervals are also constructed based on the 5% and 95% ranks of the experimental data [22].

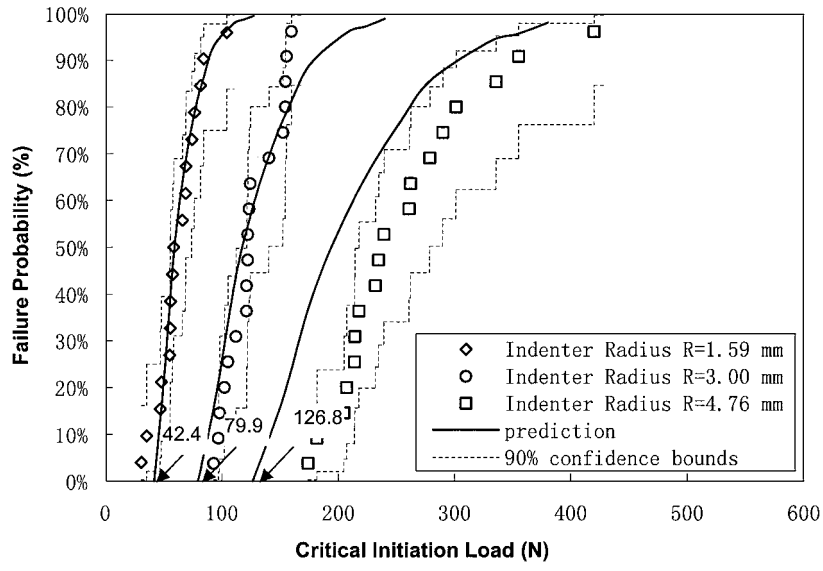

Figure 6 Probability of failure distribution: discrete points are experimental results; lines are analytical results. Three sets of data are presented for 3 different sizes of indenter ball as indicated.

The theoretical predictions match the experimental results very well for indenter ball radii 1.49 mm and 3.00 mm. For indenter ball radius 4.76 mm, the theoretical curve shifts to the left relative to the experimental data. Generally speaking, the predictions are satisfactory.

4.2.3. Discussion of indentation tests

In the theoretical methods described in section 2, both the minimum critical fracture initiation load and the failure probability predictions are based on the axisymmetric analysis. Therefore, the initiation of an axisymmetric ring crack is implicitly assumed in the analysis. This requires axisymmetric distribution of the initial flaws of various depths on the sample surface leading to an instantaneous initiation of the axisymmetric ring crack. When the indenter ball size is very small, the actually initiated crack shape is close to the axisymmetric cone since the crack precursors quickly develop to be an axisymmetric ring crack. However, the initial cracks for larger ball sizes are often not perfect axisymmetric ring cracks, and therefore additional surface energy is required to create an axisymmetric ring crack from the initial crack precursors. Therefore, the model based on the assumption of axisymmetric distribution of the crack precursors predict smaller failure loads than the actual experimental results.

5. Discussion of model applicability to failure prediction

Fisher-Cripps [12] combined the statistical approach with the fracture energy balance model as summarized in section 2. However, in comparing the theoretical predictions against their experimental results, a factor, β, was introduced into the theory in order to adjust their estimation of surface energy to the known value of surface energy. They argued that this factor, β, accounted for the friction between the indenter and the specimen, citing the work by Johnson *et al*. [21].

However, in the experimental results by Argon *et al*. [5], no significant difference in fracture load was observed in the comparative tests with lubricated and unlubricated indenters. Also Fisher-Cripps' own experimental results show no significant difference for lubricated and unlubricated spherical indenters. Johnson *et al*. [21] commented that the cleaning technique used by Argon *et al*. [5] was not sufficiently rigorous to raise the coefficient of friction above the "boundary lubrication" value of 0.10 to 0.15 and thus all their tests can be considered as done under lubricated conditions. If indeed, the effect of friction change was not observable in the "lubricated" and the "unlubricated" experiments, it implies that the effect of friction for tests with spherical hard indenters is very small if not negligible. Therefore, it raises questions as to the validity of the argument that the empirical parameter β can be attributed to friction.

In the present work, we find that this additional factor, β, does not appear to be necessary. It is important to note that the theoretical predictions shown in Fig. 6 were produced solely based on the measured Weibull parameters and Poisson's ratio.

The major difference between our experiments and those of Fischer-Cripps and Collins [11] and Fischer-Cripps [12] is that, in this work, the Weibull parameters were determined experimentally by biaxial flexural tests performed on samples with identical surface conditions as those used for the surface indentation tests. In previous investigations [11, 12], the Weibull parameters were taken from the literature, and therefore, the specimen surfaces may not have been identically prepared. (Our own experiences show that the consistent sample surface preparation is critical for the repeatability of such experimental data). Also, since crack initiation is determined by optical methods, the resolution of crack detection may vary from one method to another. Clearly, our data resulted in lower crack initiation loads than those reported by Fischer-Cripps for similar glasses [12]. In our work crack initiation was determined using a method that differed from those reported previously [11, 12]. The different methods of observation and sensitivities to crack detection may explain the generally lower initiation loads observed.

Additional differences may arise from the Poisson's ratio determination. A set of ϕ curves in Fig. 3 is significantly influenced by the value of the Poisson's ratio. A small difference in Poisson's ratio leads to a large difference in the calculated value of the constant ϕ_a. The elastic properties of glasses can vary from manufacturer to manufacturer and should be determined experimentally for a given batch of samples. In our experiments, Poisson's ratio was measured ultrasonically. In previous investigations [11, 12] the method of determining Poisson's ratio was not specified and an average value reported from the literature may have been used.

In summary our experiments demonstrate that the theoretical model proposed by Fischer-Cripps and Collins [11] and Fischer-Cripps [12] does not need the addition of an empirically derived parameter and can be used as a predictive tool for failure probability analysis in indentation tests.

6. Conclusions

In this work, we applied the theoretical model developed by previous investigators [11, 12] to predict indentation tests results for a borosilicate glass. The elastic moduli of the specimens were determined using ultrasonic methods. The Weibull parameters were experimentally determined by biaxial tests using specimens with the same surface condition as in indentation tests.

The comparison between the theoretical prediction and experimental data demonstrates an excellent match for small indenter ball sizes without using any fitting parameters. The comparison between the theoretical prediction and experimental data for larger indenter ball sizes demonstrates a slight shift of the theoretical prediction towards smaller values. The difference may be attributed to the assumption in the model of axisymmetric flaw shape. In general, we obtain good agreement between the theoretical predictions and experimental data. The current work further reinforces the theoretical

model developed previously [11, 12] indicating that it can be used as a predictive tool and possibly be extended to other applications.

Acknowledgments

This research was supported by the Ohio State University Interdisciplinary Biomaterials Seed Grants.

Appendix A: Hertz-Huber stress field

The axisymmetric stress field for Hertz spherical indentation on a semi-infinite space, known as the Hertz-Huber stress field is summarized as follows.

$$\sigma_{\theta\theta}/p_{\mathrm{m}} = -\frac{3}{2} \times \left\{ \begin{array}{l} \dfrac{1-2\nu}{3}\dfrac{a^2}{r^2}\left[1-\left(\dfrac{z}{\sqrt{u}}\right)^3\right]+\left(\dfrac{z}{\sqrt{u}}\right) \\ \quad \times\left[2\nu+u\dfrac{1-\nu}{a^2+u}-(1+\nu)\dfrac{\sqrt{u}}{a}\arctan\left(\dfrac{a}{\sqrt{u}}\right)\right] \end{array} \right\}$$

$$\sigma_{\mathrm{rr}}/p_{\mathrm{m}} = \frac{3}{2} \times \left\{ \begin{array}{l} \dfrac{1-2\nu}{3}\dfrac{a^2}{r^2}\left[1-\left(\dfrac{z}{\sqrt{u}}\right)^3\right]+\left(\dfrac{z}{\sqrt{u}}\right)^3\dfrac{a^2u}{u^2+a^2z^2} \\ \quad +\dfrac{z}{\sqrt{u}}\left[u\dfrac{1-\nu}{a^2+u}+(1+\nu)\dfrac{\sqrt{u}}{a}\arctan\left(\dfrac{a}{\sqrt{u}}\right)-2\right] \end{array} \right\}$$

$$\sigma_{\mathrm{zz}}/p_{\mathrm{m}} = -\frac{3}{2}\left(\frac{z}{\sqrt{u}}\right)^3\left(\frac{a^2u}{u^2+a^2z^2}\right)$$

$$\tau_{\mathrm{rz}}/p_{\mathrm{m}} = -\frac{3}{2}\left(\frac{rz^2}{u^2+a^2z^2}\right)\left(\frac{a^2\sqrt{u}}{a^2+u}\right)$$

where

$$p_{\mathrm{m}} = P/\pi a^2$$

is the mean contact pressure, and

$$u = \frac{1}{2}\left\{(r^2+z^2-a^2)+\sqrt{(r^2+z^2-a^2)^2+4a^2z^2}\right\}.$$

References

1. H. HERTZ, *J. Reine Angew. Math.* **92** (1881) 156; "Translated and Reprinted in English in 'Hertz's Miscellaneous Papers'" (Macmillan & Co., New York, 1896) Ch. 5.
2. H. HERTZ, *Verhandlungen des Vereins zur Beforderung des Gewerbe Fleisses* **61** (1882) 449; "Translated and Reprinted in English in 'Hertz's Miscellaneous Papers'" (Macmillan & Co., New York, 1896) Chap. 6.
3. F. AUERBACH, *Annalen der Physik und Chemie Poggendorff* (Leipzig) **43** (1891) 61.
4. J. P. A. TILLETT, *Proc. Phys. Soc.* B **69** (1956) 47.
5. A. S. ARGON, Y. HORI and E. OROWAN, *J. Amer. Ceram. Soc.* **43**(2) (1960) 86.
6. B. HAMILTON and H. Rawson, *J. Mech. Phys., Solids* **18** (1970) 127.
7. M. T. HUBER, *Ann. d. Phys.* **43** (1904) 61.
8. K. L. JOHNSON, "Contact Mechanics" (Cambridge University Press, Cambridge, 1985).
9. F. C. FRANK and B. R. LAWN, *Proc. Roy. Soc.* A **299** (1967) 291.
10. R. MOUGINOT and D. MAUGIS, *J. Mater. Sci.* **20** (1985) 4354.
11. A. C. FISCHER-CRIPPS and R. E. COLLINS, *ibid.* **29** (1994) 2216.
12. A. C. FISCHER-CRIPPS, *J. Mater. Sci.* **32** (1997) 1277.
13. S. B. BATDORF and J. G. CROSE, *J. Appl. Mech.* **41** (1974) 459.
14. S. B. BATDORF and M. L. HEINISCH JR, *J. Amer. Ceram. Soc.* **61**(7/8) 355.
15. W. G. BROWN, "A Load Duration Theory for Glass Design" (National Research Council of Canada, Division of Building Research, Ottawa, Canada, 1972).
16. A. G. EVANS, *J. Amer. Ceram. Soc.* **61**(7/8) (1978) 302.
17. L. Y. CHAO and D. K. SHETTY, *ibid.* **73**(7) (1990) 1917.
18. L. Y. CHAO and D. K. SHETTY, *ibid.* **74**(2) (1991) 333.
19. S. M. WIEDERHORN etc., *ibid.* **57** (1974) 336.
20. S. M. WIEDERHORN, etc., in "Fracture Mechanics of Ceramics," Vol. 2, edited by R. C. Bradt, etc. (Plenum, 1974) p. 829.
21. K. L. JOHNSON, J. J. O'CONNOR and A. C. WOODWARD, *Proc. R. Soc. Lond.* A 334 (1973) 95.
22. B. DODSON, "Weibull Analysis" (ASQ Quality Press, Milwaukee, Wisconsin, 1994) p. 66.

Received 21 October 2002
and accepted 16 January 2003